Soft Matter

PAPER

View Article Online
View Journal | View Issue

Cite this: *Soft Matter*, 2024, **20**, 7692

Controlling the size and elastic modulus of in-aqueous alginate micro-beads

Jean Cappello, †*[ab] Jonas Miguet, †[a] Adrien Dewandre,[c] Lucie Ergot,[d] Sylvain Gabriele,[d] Jean Septavaux[c] and Benoit Scheid[a]

Received 28th February 2024,
Accepted 5th September 2024

DOI: 10.1039/d4sm00260a

rsc.li/soft-matter-journal

The fabrication of microgels, particularly those ranging from tens to hundreds of micrometers in size, represents a thriving area of research, particularly for biologists seeking controlled and isotropic media for cell encapsulation. In this article, we present a novel and robust method for producing structurally homogeneous alginate beads with a reduced environmental footprint, employing a co-flow focusing microfluidic device. These beads can be easily recovered in an oil-free aqueous medium, making the fabrication method highly suitable for diverse applications. We demonstrate precise control over the production of perfectly spherical beads across a wide range of diameters, from about 30 to 300 μm. We then measure Young's moduli of the beads, revealing a wide accessible range from 90 Pa to 11 kPa, contingent upon controlling the type (*e.g.* chain length) and concentration of alginate.

1 Introduction

In the past decade, hydrogels have attracted considerable attention, essentially due to their ability to reproduce intra- and extra-cellular environments in the context of artificial cell development.[1] Of particular interest, alginate, a natural polysaccharide extracted from brown seaweeds, is certainly one of the most used biopolymers to produce hydrogels for this application.[2–4] Other applications in numerous and diverse areas, ranging from the pharmaceutical research[5,6] to the food science[6,7] or the cosmetics[6] and paint[8] industries were also reported for these alginate-based microgels. As a novel application, these beads, if well controlled in size and in elasticity, would serve as model systems for designing cell sorting strategies in microdevices when only the deformability can be used as a discriminating factor, as it was already demonstrated for deformable drops using inertial microfluidics.[9]

Production of alginate beads relies on the generation of droplets of aqueous alginate solution that gelifies when interacting with divalent cations such as Ca^{2+}. Different techniques have been developed for the generation of alginate droplets. Bulk emulsification,[10] electrostatic dripping,[11] vibrating nozzle,[12] spinning disk[13] or jet cutter[14] are some of the different options avalaible at the macro-scale.[15] However, besides requiring complex manipulation or specific equipment,[15] these techniques come along with major drawbacks such as poor control over the shape and structural homogeneity of the beads, a large size (millimeter scale) and size distribution, and low generation frequency.

These limitations can be overcome with the help of microfluidic tools that enable the production, in an immiscible continuous phase, of highly monodispersed micron-size droplets, with high throughput. Microfluidic droplet generators using either T-junction,[16–18] cross-flow,[19–23] co-flow[24] or flow-focusing[2,25–27] geometries can be used to generate droplets of an alginate solution in an oil phase. Droplet generation is followed by the alginate crosslinking that occurs when the droplets interact with divalent cations. To avoid the clogging of the device, it is necessary to include a time lag between the droplet generation and the gelation process. Different strategies have been proposed for this purpose. One of them consists in bringing calcium cations in the oily continuous phase through another inlet located downstream the alginate droplet generation, and thus initiating the gelation at a specific location.[28,29] A second strategy relies on bringing an aqueous solution of calcium chloride directly into contact with the alginate droplet. It can be achieved by generating droplets of alginate and droplets of calcium chloride solution in an oily continuous phase and inducing coalescence of the two aqueous droplets, thus triggering the gelification of alginate, downstream the channel.[21,30–32] The main disadvantage of this technique is the poor control over the bead shape and the structural homogeneity of the microgels.[3,25,31] Ahmed *et al.* overcame these drawbacks by releasing the calcium chloride solution directly inside the alginate droplet (Fig. 1(a)).[2] In all

[a] *Transfers, Interfaces and Processes, Université libre de Bruxelles, CP165/67, 1050 Brussels, Belgium. E-mail: jean.cappello@ulb.be*
[b] *University of Lyon, Université Claude Bernard Lyon 1, CNRS, Institut Lumière Matière, F-69622 Villeurbanne, France*
[c] *Secoya Technologies, 1348 Louvain-la-Neuve, Belgium*
[d] *Mechanobiology & Biomaterials Group, Research Institute for Biosciences, CIRMAP, University of Mons, 20 Place du Parc, Mons B-7000, Belgium*
† The two first authors contributed equally to this work.

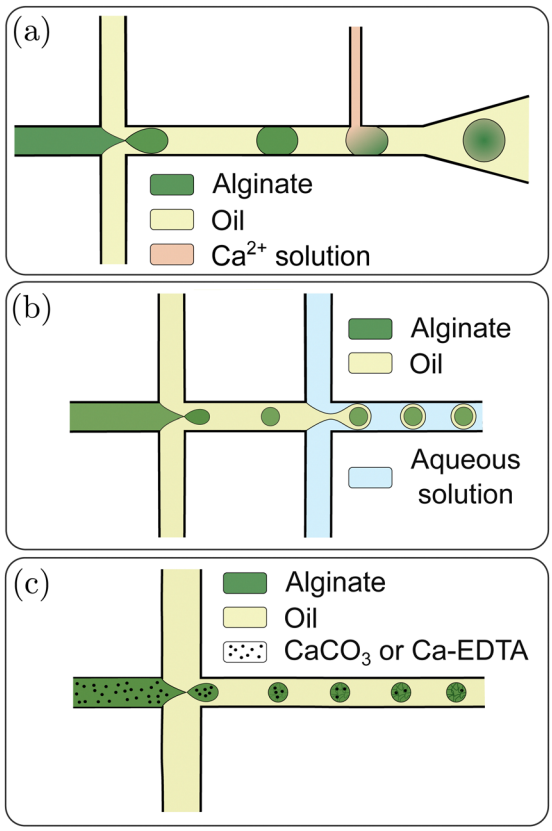

Fig. 1 Existing fabrication methods. (a) Addition of calcium cations to the alginate droplets: after production of droplets of alginate in oil, a T-junction is used to inject $CaCl_2$ into the droplet to trigger the alginate gelation.[2] (b) Shielding techniques: double emulsion of alginate/oil/water is produced. Gelation is triggered either "on-chip" by adding calcium cations in the aqueous solution,[22] or "off-chip" by adding the calcium in the recovered suspension.[23] (c) pH-triggered gelation: calcium carbonate,[19,35] or Ca–EDTA[25,26] is added to the alginate phase. Upon acidification of the medium, calcium ions are released and gelification starts. Gelation can occur "on-chip"[35] by acidifying the continuous phase, or "off-chip" by acidifying the recovered emulsion.[19,25,26]

the aforementioned fabrication methods, alginate microbeads are generated in an oily phase, which might be undesirable in some applications such as cell-encapsulation since the presence of the oil as a continuous phase is incompatible for long term cell culturing as it prohibits nutrient exchanges[33,34] and thus makes necessary the use of an additional and challenging oil removal process.[3]

The use of double emulsion droplets with a core of alginate, and an oil shell, in an aqueous continuous phase appears as a promising alternative to reduce the amount of organic components. Such solutions have been proposed by Saeki *et al.*[22] and Liao *et al.*[23] In both studies, two consecutive cross-junctions are used to fabricate droplets of alginate with a thin shell of oil transported in an aqueous external phase (Fig. 1(b)). Then, gelation is induced either "off-chip" by the addition of a sodium chloride solution to the recovered double emulsion suspension[22] or "on-chip" by the use of calcium chloride solution as a continuous phase.[23,24] In both cases, calcium diffuses through the oil shell leading to a gentle hydrogel crosslinking. Gelation is followed by a spontaneous detachment of the oil shell leaving the microgels in the aqueous solution and allowing for an easy removal of the oil phase. However, these recent approaches lead to inhomogeneous gelation and consequently a variation of the gel elastic properties between the center and the edge of the beads.[3]

Currently, the technique that offers the best structural homogeneity of the alginate gel relies on the suspension, directly in the alginate solution, of a gelation reagent, that can be calcium carbonate ($CaCO_3$)[19,20,35] or other synthesized complexes, such as calcium–ethylenediaminetetraacetic acid (Ca–EDTA),[25,26] which releases Ca^{2+} ions in a specific pH range and hence induces alginate gelation (Fig. 1(c)). Calcium carbonate being insoluble in aqueous solution, $CaCO_3$, is added to the alginate solution in the form of nanoparticles making $CaCO_3$ a bad candidate for cell encapsulation as physical contact between the nanoparticles and the cell decreases their viability.[19] This problem is not encountered when using Ca–EDTA that dissolves better into water. At pH above 6, Ca^{2+} are chelated by EDTA and do not interact with the alginate chains. Hence, a perfectly homogeneous mixture of alginate and chelated ions can be obtained without inducing gelation. Acidification of the solution leads to the release of the cations and thus to the homogeneous gelation of the alginate.[25] Benefitting from these properties, structurally homogeneous alginate beads can be achieved by generating droplets of a premixed alginate–Ca–EDTA solution in an oil phase using a microfluidic flow-focusing device. After droplet formation, gelation is induced by adding acetic acid to the oil phase either "off-chip"[25] or "on-chip" by means of an additional inlet downstream where acidified oil is introduced.[26] However, alginate beads are recovered in an oil medium, thus requiring an additional step for oil removal. Moreover, the oil used in ref. 25, namely HFE-7500, is volatile, with a global warming potential of 12 over a time range of 100 years[36] – probably significantly more if the synthesis is included – and has potential effects on wildlife and human health.[37]

In this article, by combining different approaches, we propose a novel method for the fabrication of structurally homogeneous alginate beads directly in an aqueous medium with cost-effectiveness and reduced environmental impacts. Similar to the studies of Saeki *et al.*[22] and Liao *et al.*,[23] we propose to reduce the amount of oil by generating a double emulsion of premixed alginate + Ca–EDTA complex solution with an oil shell (oleic acid) in an acidified aqueous solution. The role of the oil shell is threefold: it enables the formation of an alginate solution droplet, serves as a shielding phase to prevent the clogging of the alginate inlet, and induces a smooth gelation as the acid has to diffuse through the thin shell to induce crosslinking. After gelation, the oil shell spontaneously detaches from the hydrogel beads leading to a direct contact between the bead and the aqueous solution and an easy removal of the oil. We show that this fabrication method allows fabricating beads of different diameters by varying the flow rate of the three phases and/or changing the geometry of the double emulsion

generator. Size distribution and circularity of the generated beads are discussed. Furthermore, by measuring the Young's modulus of microgels obtained from different alginate solutions, we show that the elastic modulus of the microgel can be tuned over more than two orders of magnitude.

2 Experimental section

2.1 Materials

All aqueous solutions are prepared with ultrapure water (Arium Pro UV, resistivity of 18.2 MΩ cm). References given for the other chemicals correspond to Merck's catalog from which they were purchased, unless specified otherwise.

The continuous phase consists of a 1 wt% acetic acid aqueous solution prepared from a stock solution of concentration 1 M (Titripur®ref. 1.60305) to which 1 wt% of polyvinyl alcohol (PVA, molecular weight of 9–10 kg mol^{-1}, 80% hydrolyzed, ref. 360627) is added to prevent coalescence of oil droplets. Typical total volumes are 100–200 mL. After adding PVA, the solution is stirred for at least 20 minutes. Pure oleic acid (ref. 364525) is used as a shell phase. The core phase consists of a solution of 1 wt%, 1.5 wt% or 2 wt% of alginic acid sodium salt to which 0.1 M of ethylenediaminetetraacetic acid calcium disodium salt hydrate (CA–EDTA, ref. ED2SC) is added. This concentration is chosen to optimise the crosslinking efficiency,[25] as detailed below. Products are dissolved in water for 20 minutes with magnetic stirring. Experiments are performed using either low viscosity (ref. A1112) or medium viscosity (ref. 180947) alginic acid sodium salt. For the sake of clarity, the label LV (MV) is used to specify that the low (medium) viscosity alginic acid sodium salt is used in the experiments. These are polysaccharides, refined from brown seeweeds,[38] and are composed of two elementary units: mannuronate (M) and guluronate (G), making them copolymers. The "low" and "medium" viscosity of our products essentially relies on the chain lengths selected by the extraction process. The molar masses, provided by the supplier, are 30–100 kg mol^{-1} and 120–190 kg mol^{-1} for LV and MV, respectively. The M/G ratio, defined as the number of M monomers per unit G, that can have an important impact on the physical properties of the gels,[3,39,40] is 1.56 for MV (supplier information). To assess the microbead's structural homogeneity, experiments using a core phase of 0.5 wt% FITC-labelled alginate (alginate fluorescein, low viscosity 100–300 cP, Creative PEGWorks, ref. AL-500) and 0.1 M of Ca–EDTA are also performed.

Following Djema *et al.*,[41] we assume that a complete gelification of the alginate is obtained when at least one Ca^{2+} cation is available for each pair of guluronates in the alginate. Defining $[Ca^{2+}]_c$ as the necessary molar amount of Ca^{2+} to achieve a complete gelation, and since by definition $M + G = 1$, we have:

$$[Ca^{2+}]_c = \frac{[G]_{\text{mol L}^{-1}}}{2} = \frac{\frac{1}{1 + M/G}[\text{alg}]_{\text{g L}^{-1}}}{2M_{G,w}}, \qquad (1)$$

where $[G]$ is the molar concentration of G for a given alginate mass concentration [alg] and $M_{G,w}$ = 216.12 g mol^{-1} is the guluronate molar mass. The measured pH of the continuous phase is 3.2 and we therefore expect a dechelation of Ca–EDTA typically superior to 40%.[41] Taking M/G = 1.56 and $[\text{alg}]_{\text{g L}^{-1}}$ = 20 g L^{-1} (corresponding to 2 wt% of alginate), we need $[Ca^{2+}]_c$ = 0.018 M. With a dechelation of 40% and an initial concentration of Ca–EDTA of 0.1 M, we can conclude that we have at least 0.04 M of Ca^{2+} and therefore complete gelation of the alginate is obtained in our experiments.

Table 1 Physical properties of the different core solutions (colors), shell phase (light grey) and continuous phase (dark grey) at 25 °C

Solution	ρ (kg.m^{-3})	η (mPa.s)
Low Viscosity 1% + 0.1M Ca-EDTA	1.023	6.3
Low Viscosity 1.5% + 0.1M Ca-EDTA	1.024	9.5
Low Viscosity 2% + 0.1M Ca-EDTA	1.028	18.6
Medium Viscosity 1.5% + 0.1M Ca-EDTA	1.023	11.4
Medium Viscosity 1% + 0.1M Ca-EDTA	1.023	24.9
Medium Viscosity 2% + 0.1M Ca-EDTA	1.028	52.3
Oleic Acid	0.891	32.45
1% PVA + 1% Acetic Acid	1.0004	1.33

Liquid properties used for the three different phases are reported in Table 1. Low-shear viscosities are measured using a rheometer (Anton Paar, MCR 302 A) equipped with a cone-plate geometry, and densities are measured by means of a densimeter (DMA 4500 M, Anton Paar). The viscosities as a function of the shear rate are further detailed in Appendix A.

The following considerations on the environmental impact of the process may be drawn. Although controversial,[42] the biodegradability of PVA, which is derived from acetylene and acetic acid, is likely ensured under the proposed working conditions.[43] At the low concentration used here, acetic acid, the main constituent of vinegar, is not detrimental when spread in the environment. It is usually obtained by methanol carbonylation.[44] Oleic acid, the main constituent of olive oil, is both of biological origin and biodegradable.[45] EDTA is the most problematic compound of the proposed method as only very specific bacterial environments allow for a proper degradation of this molecule.[46] A further improvement of the proposed method would be to replace this product with other, more sustainable, chelating agents, but it is beyond the scope of this work.

2.2 Fabrication of alginate microgels

The production of alginate beads can be divided into three distinct steps, as illustrated in Fig. 2. The first one consists of the generation of a double emulsion of an aqueous solution of Ca–EDTA + alginate, surrounded by a shell of oleic acid and carried by an acidified aqueous phase containing surfactants (Fig. 2(a) and (b)). The second step corresponds to the gelation and collection of the alginate beads (Fig. 2(c)–(e)), and the third one is the oil separation and recovery of beads (Fig. 2(f)–(h)).

2.2.1 Generation of the double emulsion. As shown in Fig. 2(b), the microfluidic chip consists of a commercially available double-emulsion droplet generator with a non-

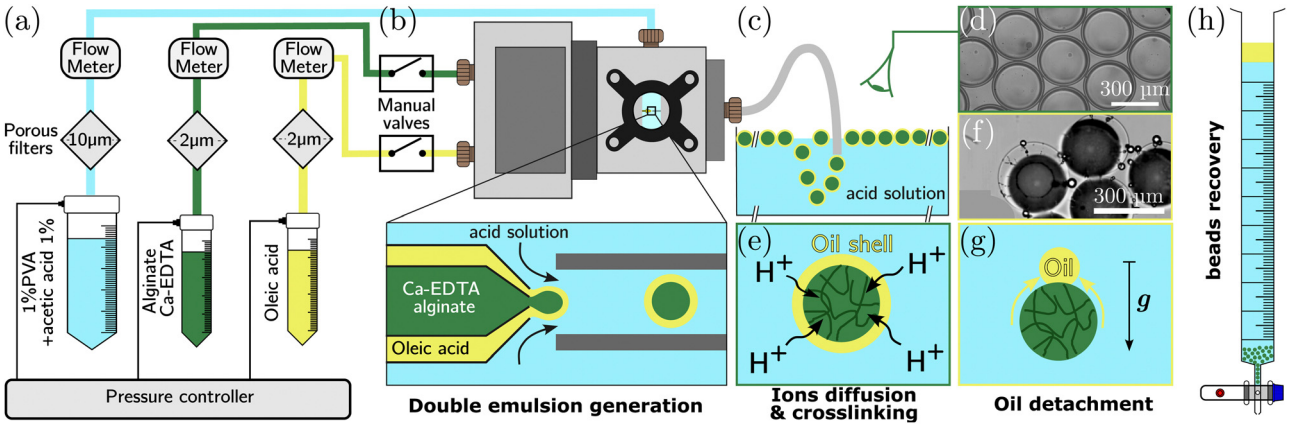

Fig. 2 Experimental procedure. (a) A pressure controller is used to impose the flow of the core (green), shell (yellow) and continuous (blue) phases, through (b) the Raydrop double emulsion generator. (c) and (d) The double emulsion is recovered in a Petri dish filled with the acidic continuous phase. (e) Once the double emulsion is generated, acid diffuses through the oil shell, from the continuous to the core phase, inducing the release of Ca^{2+} cations already present in the alginate solution but initially chelated by EDTA, leading to the gelation of the alginate. (f) and (g) As gelation occurs, a spontaneous detachment of the oil shell is observed. (f) The picture shows a bottom view of the detached oil (dark gray disks) and the beads (transparent disks with black interfaces located bellow the oil droplets) while (g) illustrates a side view of the oil drainage. (h) After oil detachment, the recovered solution is placed into a burette. Alginate beads being heavier than the continuous phase which is heavier than the oil, they sediment at the bottom of the burette while the oil droplets migrate to the top. Hence, opening the burette allows both to recover concentrated beads suspended in an aqueous solution and to get rid of the oil.

embedded co-flow-focusing geometry[47,48] (Raydrop Double Emulsion, Secoya). Compared to a microfluidic droplet generator presented by Dewandre *et al.*,[47] in the present study, we used a 3D-printed nozzle consisting of the constriction of two coaxial outlets[49] (see Fig. 2(b)). The core phase is transported through the inner outlet while the shell phase passes through the outer outlet. The continuous phase is flown in the pressurized chamber that has a typical size of 1 cm towards the extraction capillary having a typical inner diameter of the order of a few hundred microns that is located in front of the nozzle. In between the nozzle and the extraction capillary, a strong axisymmetrical acceleration of the continuous phase takes place inducing viscous forces at the shell interface that allow for the detachment of the core and shell phases from the nozzle. By this method, a double emulsion is generated and is transported through the extraction capillary. In order to sweep a broader range of sizes for the produced double emulsions, two configurations of the nozzle and extraction capillaries were used: a small nozzle (SN) configuration, having an extraction capillary with 150 µm inner diameter, a core outlet diameter of 30 µm and a shell outlet diameter of 70 µm and a large nozzle (LN) configuration, having a dimension of 450 µm for the extraction capillary inner diameter and a core and shell outlet diameters of 90 µm and 160 µm, respectively.

Pressure controllers (MFCS-EX, MFCS-EZ or Flow EZ, Fluigent), coupled with flow meters (FLOW UNIT from Fluigent or Coriolis M12 from Bronkhorst) are used to flow the three phases and monitor the flow rates (Fig. 2(a)). Each phase is connected to the Raydrop device by standard HPFA tubings (IDEX Health & Science) and passes through a porous filter of 10 µm porosity (continuous phase) or 2 µm porosity (shell and core phases). Additional manual valves are used to avoid undesired back-flows of the core and shell phases. The microfluidic chip is mounted on an optical microscope (Eclipse Ti, Nikon) connected to a fast camera (IDT Y3 Motionpro) allowing to visualize the double emulsion production and measure the generation frequency.

It is important to avoid direct contact between the continuous phase and the core phase in the microfluidic system because this would result in internal gelation and potentially clogging of the nozzle. Hence, a typical experiment consists first in setting the flow of the continuous phase directly towards the extraction capillary, keeping the core and shell pipes closed. The shell phase (oleic acid) is then opened until a simple emulsion of oleic acid in the continuous phase is produced. At this stage, the core phase flow is started and the double emulsion is produced with the oil playing the role of a shield preventing direct contact between the core and continuous phases. Varying the flow rates of the three phases enables tuning (i) the double emulsion size, (ii) the thickness of the shell and (iii) the generation frequency. (i) The size of the double emulsion, and hence of the resulting alginate beads, can be modified by adjusting the flow rate of the continuous phase (Q_c) while keeping the other two flow rates constant – the larger the continuous phase flow rate the smaller the double emulsion –. (ii) The thickness of the shell, for an identical core size, depends on the flow rate imposed on the shell phase (Q_s) – the larger the shell phase flow rate the larger the shell thickness –. (iii) The generation frequency can be increased by simultaneously increasing the flow rates of the dispersed phase (Q_d) and the shell phase (Q_s). Table 2 summarizes the flow rates of the three phases used to generate various alginate beads.

2.2.2 Gelation and collection. The association constant of calcium ions with EDTA at neutral pH is significantly higher than that with alginate, preventing crosslinking. As soon as the double emulsion is formed, acid diffuses through the oleic acid shell from the acidic continuous phase towards the core.

Table 2 Bead size distributions and experimental conditions. Flow rates of the continuous (Q_c), shell (Q_s) and dispersed alginate core (Q_d) phases are given for different experiments. The labels are constructed as follows: the prefix indicate the nozzle type (SN: small nozzle; LN: large nozzle). It is followed by the experiment number (with the exception of J that corresponds to a jetting regime as explained further). Then the wt% values of alginate and the alginate type are specified (LV: low viscosity; MV: medium viscosity). The frequency (f) and the diameter of beads with standard deviation (d_b) and circularity (CV) are also indicated

Label	Q_c μL.min^{-1}	Q_s μL.min^{-1}	Q_d μL.min^{-1}	f Hz	d_b μm	CV
SNJ 1% LV	696	5.4	10	8100	34±5	1.00±0.05
SN1 1% LV	391	2.8	3.8	387	60±5	1.03±0.03
SN2 1% LV	163	0.8	2.9	92	111±7	0.95±0.07
SN3 1% LV	120	2.4	8.2	203	120±3	0.89±0.07
LN1 1% LV	5010	19	24	234	123±8	0.95±0.07
LN2 1% LV	680	34	10	41	152±8	0.95±0.07
LN3 1% LV	1830	10	5.6	32	235±14	0.90±0.09
LN4 1% LV	991	45	99	105	311±7	0.89±0.06
LN 1.5% LV	1096	34	73	93	281±5	0.99±0.02
LN 2% LV	1910	30	25	110	242±13	0.88±0.08
LN 1% MV	2140	12	15	42	216±9	0.92±0.07
LN 1.5% MV	1087	31	70	87	289±5	0.97±0.03
LN 2% MV	1750	17	11	52	183±9	0.98±0.04

Upon protonation of EDTA, its association constant with calcium drops, leading to the release of calcium made available for crosslinking. We typically found that above pH 4.5 no gelation is observed while pH 4 yields crosslinked beads.

Before collecting the double emulsion droplets, a first verification step improves the reliability of the process. A few tenths or hundreds of double emulsion droplets are recovered in a glass watch prefilled with a small amount of acidified continuous phase (see Fig. 2(d)) in order to verify the integrity of the double emulsions when they reach the exit of the set-up. Moreover, it allows observing the spontaneous detachment of the oil shell occurring while alginate gelifies and measuring the lifetime of the double emulsion, defined as the time elapsed between double emulsion fabrication and shell detachment from the bead. This time needs to be high enough to ensure that a sufficient amount of acid has penetrated into the core to release the Ca^{2+} ions from the EDTA structure to trigger the gelation (Fig. 2(e)). If this time is too short, the direct contact of the core and continuous phases either leads to dissolution of the core in the continuous phase, or to poorly spherical beads (typically featuring invaginations or tear shapes). The relevant time is usually anything above 5 minutes. We observed that the thicker the shell, the shorter the lifetime, which is why all experiments feature rather thin shells. Once this verification is performed, the collection *per se* can start. We preferably use a disposable plastic Petri dish to avoid wetting of the beads on the surface. A glass capillary (Fused Silica, Postnova) connects the Raydrop to the Petri dish (Fig. 2(c)). We match the inner diameter of the glass capillary to the one of the extraction capillary of the Raydrop in order to avoid section jumps and possible collapse of the double emulsions. A small amount of the continuous phase in the Petri dish can be used to avoid drying or overlapping of the double emulsions prior to the oil detachment. During collection, it is also recommended to slowly shake the Petri dish from time to time, to avoid double emulsion overlapping. A cover may be placed at the top of the Petri dish to limit evaporation and pollution of the sample. Depending on the frequency of generation and on the flow rates, this step typically lasts a few tens of minutes. When the collection is done, the glass capillary is removed from the Petri dish and we wait an additional 10 minutes to allow oil shell detachment from the alginate beads (Fig. 2(f) and (g)).

2.2.3 Separation and recovery. The separation of the oil from the core phase and the recovery of the alginate beads rely on the difference of density of the three phases (see Table 1). Indeed, as the oleic acid is lighter than the alginate, there is a drainage of the shell that eventually detaches from the core. After the oil detachment, the collected solution is placed into a burette (Fig. 2(h)). Because alginate beads are heavier than the continuous phase which is heavier than the oil, alginate beads sediment at the bottom of the burette while oil migrates to the top. Hence, by taking the first few drops from the burette, we obtain a highly concentrated suspension of alginate beads in the aqueous continuous phase, *i.e.* totally free of oil.

2.3 Post processing

After collection, pictures of the bead suspensions are taken using a bright-field microscope in order to characterize their size and shape. A Matlab routine is used to measure the diameter of beads and their circularity. The routine is composed of two consecutive steps. First, a Hough transform is used on the gray scale image to determine the position and radius of the bead (Fig. 3(a) and left panel of Fig. 3(b)). Then, around each bead, background is removed, contrast is enhanced and the image is binarized (Fig. 3(b) central panel) in order to find the contours of the beads pixel by pixel (Fig. 3(b) central and left panels). The bead circularity, CV, is then calculated with the formula:

$$\mathrm{CV} = \frac{4\pi A}{P^2}, \tag{2}$$

where P is the perimeter of the bead and A its area.

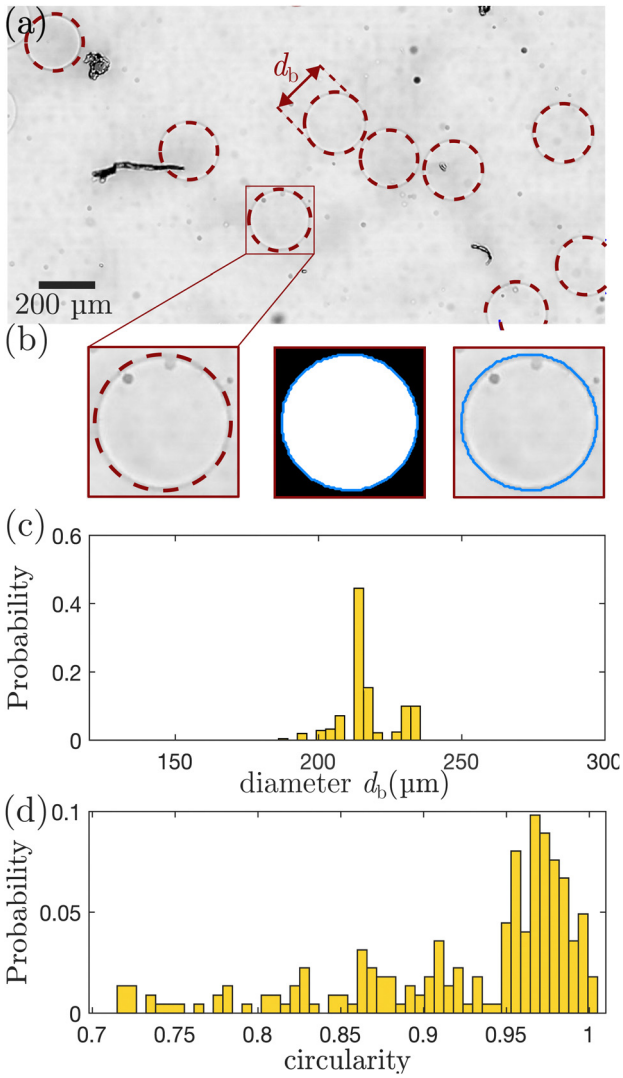

Fig. 3 A typical post processing example for LN 1% MV. (a) Bright-field microscopy image of the beads. The dotted circles correspond to the positions and sizes of the beads obtained using a Hough transform. (b) After determining the beads' positions, the image is cropped around each bead (left), each cropped image is binarized (center) and the bead contour, illustrated by the blue line, is determined (center and right). (c) Probability density function of the bead size obtained by processing several images similar to (a). (d) Probability density function of the bead circularity, CV, obtained by processing several images similar to (a).

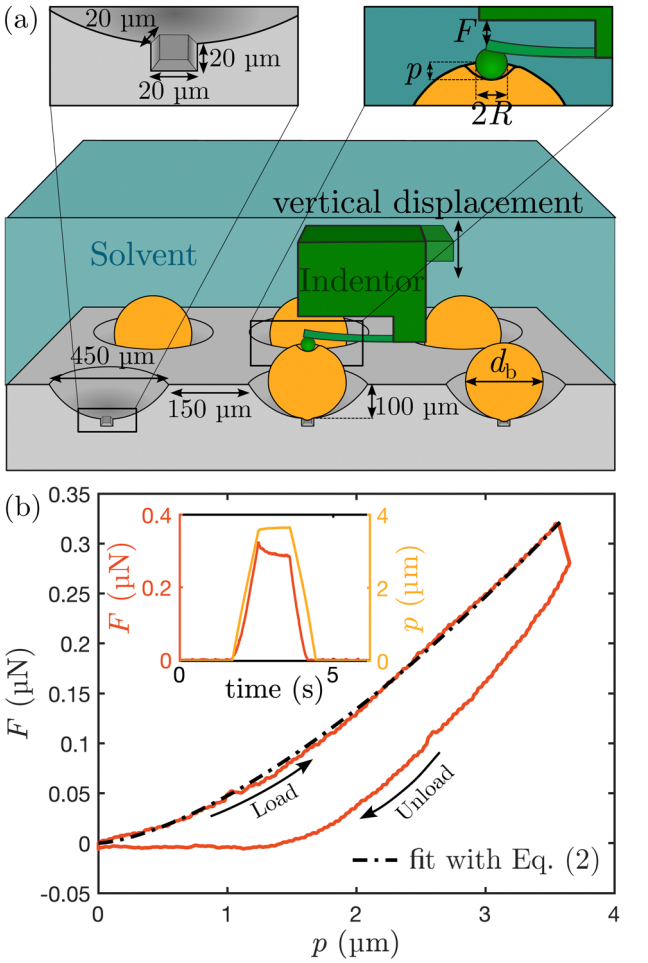

Fig. 4 Young's modulus measurements. (a) Scheme of the experimental apparatus used for the indentation of the microgels. (b) Indentation force, F, as a function of the depth of penetration, p. Inset: temporal evolution of F (red) and p (orange).

The distributions of diameter and circularity for the particular experiment shown in Fig. 3(a) are given in Fig. 3(c) and (d), respectively. For each experiment, at least 200 different beads were measured to provide statistical significance of the results. From the size distribution we define the relative error as $\Delta d_b/\bar{d}_b$ where $\bar{d}_b$ and Δd_b are, respectively, the mean and the standard deviation of the distribution.

To visualise the structural homogeneity of the alginate microbeads, a FITC-labeled alginate is used. Epi-illumination fluorescence microscopy imaging is performed using a upright microscope (Nikon Eclipse FN1), equipped with a 10× TU Plan Fluor (NA = 0.3) objective, a fluorescent filter cube (TE/FITC Ex 482/35 nm DM506 Em 536/40 nm), and a color camera (Ximea, xiC) (see Fig. 6(a) and (b)). A MatLab routine is used to average the fluorescence intensity over the azimuthal angle and obtain the mean fluorescence intensity as a function of the radial position (see Fig. 6(c) and (d)).

2.4 Young's modulus measurements

Young's moduli of the beads are measured using static micro-indentation (Chiaro Nanoindenter, Optics11 Life). Measurements are achieved with the beads immersed in water in order to take into account the effects of swelling on the mechanical properties. To prevent lateral displacement of the alginate beads we used an in-house glass slide decorated, using a femtosecond laser (FEMTOprint), with an array of etched hemispheres of radius 450 μm with an additional small hole at their centers of typical width, length and depth of 20 μm. Hence, the beads are trapped at the center of these hemispheres (see Fig. 4(a)). The Chiaro Nanoindenter system consists of a ferrule-top force transducer, comprising a micromachined cantilever spring with an optical fiber readout, mounted on a 3D-printed

holder screwed to a Z-piezoelectric actuator (PI p-603.5S2, Physik Instrumente). The single-mode fiber of the readout was coupled to an interferometer (OP1550, Optics11), where the interference signal was directly translated into cantilever deflection. The piezoelectric actuator with the probe was mounted on a XYZ micromanipulator (PatchStar, Scientifica) for the automatic mapping of the mechanical properties. A unique indentation was performed and measurements were repeated on 7 different beads for each alginate type and concentration. We employed colloidal probes with a tip diameter of 51 μm. Before testing, the sensitivity calibration of the cantilever was conducted by indenting a hard surface. During indentation, we measured the depth of penetration p together with the indentation force F. A typical F–p plot is shown in Fig. 4(b). The Hertz contact theory was used to determine the relation between the indentation force and the penetration depth during the loading regime:

$$F = \frac{4}{3}\frac{E}{1-\nu^2}p^{3/2}R^{1/2}, \quad (3)$$

where E is Young's modulus, ν is Poisson's ratio of the hydrogel and R is the radius of the indenter. Assuming incompressible hydrogels,[50] *i.e.* $\nu = 0.5$, we derived Young's modulus by fitting the force–displacement curves with the Hertz formula. As the Hertz theory describes plan-sphere contacts, we used beads of 300 μm in diameter, which were six times larger than the probe diameter.

3 Results

Fig. 5(a) shows the size distributions for all the experiments performed with low viscosity alginate 1%. The green

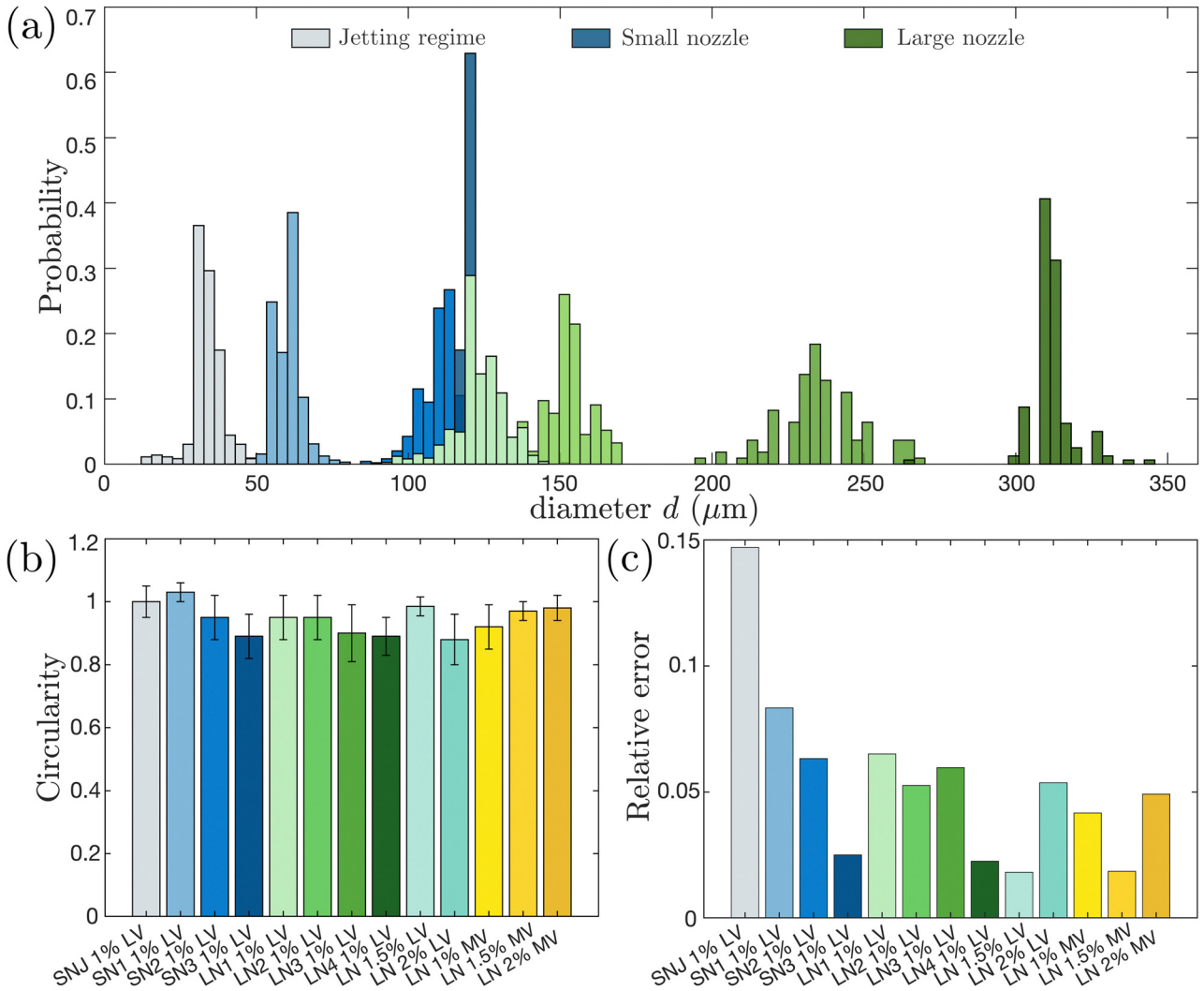

Fig. 5 Size and shape characterization. (a) Size distributions of beads generated for varying flow rates of the core, shell and continuous phases (see Table 2) with a core solution containing 1% of LV alginate. The various shades of blue (green) correspond to experiments carried out in the dripping regime using the small nozzle (large nozzle) configuration. The grey distribution corresponds to beads generated with the small nozzle in the jetting regime. (b) Circularity of the beads as defined in eqn (2), for the various experiments reported in Table 2. (c) Relative error on the bead diameter, $\Delta d_b/\bar{d}_b$, for the same experiments. The color code of (a)–(c) is the same as that used in Table 2.

distributions correspond to the large nozzle and feature typical sizes between 123 μm and 311 μm, while the blue ones correspond to the small nozzle and feature sizes spanning between 60 μm and 120 μm (see Table 2 for the standard deviations). We therefore see that the range of sizes achievable with this method is very wide. Additionally, the overlap between small and large nozzles allows in principle obtaining any size between 60 μm and 311 μm, by tuning the flow rates according to the target size.

The frequency of production is not the main scope of this work but a comparison between experiment SN2 1% LV and SN3 1% LV shows that for a given bead size, several combinations of the flow rates are possible, which can thus allow adapting the frequency of generation, even though the relation between all these parameters is not trivial. In practice, the operator can tune the flow rates while observing the resulting flow with the camera. Typically after a few minutes, a stable emulsification can be achieved with core sizes corresponding to the target value. The standard deviation reported in Table 2 is quite constant around 10 μm which corresponds to relative errors consistently inferior to 10%, as shown in Fig. 5(c), except for the grey experiment carried out in the jetting regime discussed thereafter. All the distributions properly peaked around the mean values with small standard deviations, demonstrating that the production is reasonably monodisperse.

In addition to the straightforward control of the typical size of the beads, Fig. 5(b) shows that for all the experiments conducted in this study, with varying flow rates and core compositions, the circularity was excellent, *i.e.* CV $\approx$ 1 (see Fig. 5(c)). It indicates that the gelation induced by the diffusion of acid across the oleic acid membrane before shell detachment is efficient enough to stiffen the gelating bead and prevents its deformation (invagination or elongation) when the shell retracts. Indeed when the shell detaches the beads come in direct contact with the acidic continuous phase and the gelation finishes almost instantaneously, freezing its shape. Hence, the presented method allows for the fabrication of well-controlled, perfectly spherical hydrogel beads at the micron scale, with diameters spanning across one order of magnitude. Note that, in our study, we chose to limit the maximum bead diameter to $d_b \sim 300$ μm. However, the nozzle and extraction capillaries are 3-D printed down to a micrometer resolution. It is therefore possible to increase the diameter of the extraction capillary and/or of the core and shell phases which would further increase the maximum bead diameter. Finally, we also report an additional experiment, SNJ 1% LV, for which 'J' refers to the microfluidic emulsification regime. All other experiments are performed in the dripping regime, for which the double emulsions are produced locally at the tip of the nozzle. SNJ 1% LV, on the other hand, was obtained in jetting mode, where two elongated co-flowing jets of the core and shell phases penetrate into the extraction capillary and destabilize concomitantly further downstream to produce double emulsion droplets.[47] This regime allows overcoming the lower 60 μm limitation of the dripping mode and reaching a typical size of 34 μm. The production frequency is extremely high and, as expected for the jetting mode, the monodispersity is slightly degraded as compared to the dripping mode, with a relative error of about 15%. The circularity however remains excellent. The continuity of the available sizes between 60 μm and 34 μm is likely not ensured in our working conditions. It could however be tuned by changing the geometrical parameters of the nozzle, which is beyond the scope of the present study. Moreover, we did not observe any size change or degradation of the beads over a period of time of one month. However, when stored under non-sterile conditions, we noticed a degradation of the alginate beads after typically 6 months.

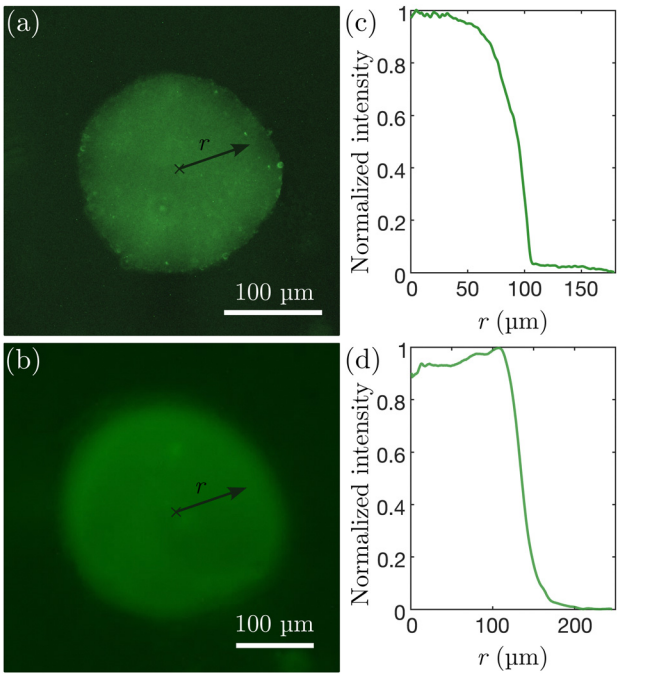

Fig. 6 Comparison of different techniques for the microfluidic fabrication of alginate microgels. A labeled alginate to achieve fluorescence was used for the illustration of the beads' structural integrity *via* fluorescent microscopy. (a) Picture of an alginate microbead fabricated using the technique described in the article. (b) Picture of an alginate mirobead crosslinked by addition of calcium ions to the continuous phase. (c) and (d) Fluorescence intensity profiles averaged over the azimuthal angle, obtained from pictures (a) and (b), respectively.

The structural integrity of the alginate microbeads is assessed through fluorescence imaging. Fig. 6(a) and (b) compare the fluorescence pictures of two beads fabricated through (a) the above mentioned technique involving the use of chelated calcium ions, and (b) a microfluidic technique involving a chelate-free approach where alginate drops are generated in oleic acid in which 1-butanol droplets containing calcium ions are suspended. In this latter case, diffusion of calcium ions from the droplet periphery toward the core leads to the alginate crosslinking. More details on the chelate-free technique – largely inspired by the study of Lian *et al.*[28] – are given in Appendix B. The intensity profiles averaged over the azimuthal angle corresponding to Fig. 6(a) and (b) are shown in Fig. 6(c) and (d), respectively. Note that the brighter small spots in Fig. 6(a) are due to small droplets of oleic acid oil that did

not properly detach from the bead. As can be seen in Fig. 6(a) and (c), using our technique, the amplitude of the fluorescence signal increases from the edges to the core of the bead as expected if homogeneous reticulation is achieved. Contrarily, when the beads are crosslinked by the technique of migration of calcium cations from the edges to the core, a maximum of the fluorescent signal close to the edge and a decrease or flattening when approaching the core (see Fig. 6(b) and (d)) is observed, meaning that crosslinking is weaker more inside the core. These results are in agreement with the study of Utech *et al.*[25] which also reports that fabrication of alginate microbeads using initially EDTA-chelated calcium leads to homogeneous microbeads. We interpret the homogeneity of the beads as a result of the initially homogeneous distribution of calcium, in its chelated form. Since protons are a much smaller chemical species than Ca–EDTA, they diffuse much faster. The release of Ca^{2+} and subsequent crosslinking of the alginate therefore occur homogeneously because the Ca–EDTA molecules are initially homogeneously distributed.

We now describe the mechanical properties of the microbeads, in terms of their Young's modulus. Fig. 7 shows the results of the indentation measurements on beads generated from different compositions of the core phase. Note that, since a complete gelification is expected (see Section 2.1) whatever the size and since it is triggered after the formation of the double emulsion droplets, we can assume that Young's modulus of the alginate beads depends only on the physicochemical properties of the Ca–EDTA alginate solution. Hence, regardless of the bead sizes or flow rates used to generate the beads, if the composition is identical, identical mechanical properties are expected. By varying the nature of the alginate (low viscosity 'LV' and medium viscosity 'MV' alginate) and the concentration (from 1 to 2 w/w%), we were able to tune the Young's modulus of the microgel over a large interval ranging from 90 Pa to 11 kPa. The Young's modulus tends to increase with the concentration for a given alginate type: the higher the concentration, the denser the polymerised matrix and the stiffer the hydrogel. On the other hand, the MV alginate, which features larger chain lengths, has Young's moduli typically one order of magnitude higher than those of the LV one. Since alginate is a natural polymer with many crosslinking sites per molecule, the longer the molecule, the less freedom is left for rearrangements under stress.

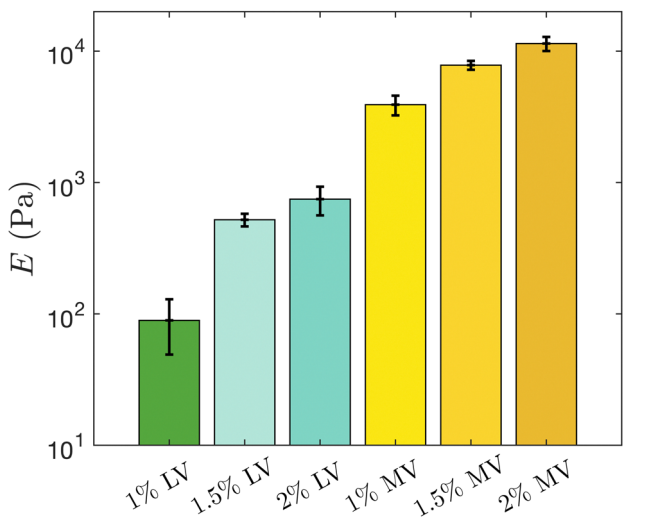

Fig. 7 Microgel mechanical characterization. Young's modulus of the various microgels generated changing the composition of the core phase. Error-bars correspond to the standard deviation measured from 7 repetitions of the measurement on different beads for each alginate type and concentration.

More notably, the elastic properties of alginate microgels align with the range of elastic properties found in soft tissues (10^2–10^4 Pa).[51] Matrix rigidity has been placed in a spotlight as one of the most significant extracellular cues. Indeed, cells actively sense the rigidity of their micro-environment and adapt their behavior accordingly.[52,53] This mechanosensing process plays a crucial role in various physiological situations, spanning from development to differentiation, and is implicated in the onset of human diseases.[54] The produced beads are therefore shown to be particularly suitable for the synthetic fabrication of model systems to study the role of a mechanical environment in cell development.

4 Conclusions

In this article, we provide a robust, environmentally friendly and versatile procedure for the production of microbeads of alginate, using double emulsions produced in a microfluidic chip. We show that all diameters between 60 μm and 311 μm can be produced with two different nozzle dimensions, with excellent monodispersity and sphericity, at least at 10–100 Hz. Smaller beads of 30 μm can be produced at an extremely high frequency (~8 kHz), with a slightly decreased monodispersity but excellent sphericity. The slow gelation process (~5 minutes), obtained through the dechelation of Ca^{2+} by a pH decrease of the alginate-containing core, ensures homogeneous mechanical properties. The Young's moduli are measured and span two orders of magnitude, around biologically compatible values. Hence, the beads can be used as realistic model systems to mimic biological objects as cells or even red blood cells while having reduced mechanical and size variability compared to these bio-objects. The beads obtained with the present method can then be used to gain a fundamental understanding of the transport of these deformable bio-objects at small scales and to potentially develop sorting strategies based on the object deformability at the microfluidic scale. Following the strategies developed recently[55,56] and enabled by cutting-edge microfabrication tools, a potential parallelization of the technique, offering a higher generation throughput, can be considered. Adaptation of the protocol to ensure biocompatibility by avoiding a long exposition to low pH, will be the focus of future works.

Author contributions

Conceptualization: J. C., J. M., A. D., and J. S.; investigation: J. C., J. M., A. D., and L. E.; data curation and formal analysis:

J. C. and J. M.; supervision: A. D., J. S., and B. S.; writing – original draft: J. C. and J. M.; writing – review and editing: all; and funding acquisition and resources: S. G., B. S., and J. C.

Data availability

All study data are included in the article. More details, and raw data that support the findings of this study, are available from the corresponding author upon reasonable request.

Conflicts of interest

The Raydrop device is manufactured and marketed by Secoya Technologies in which A. Dewandre, J. Septavaux and B. Scheid hold shares. Other authors have no competing interests.

Appendices

A Measurements of bulk viscosities

The viscosity has been measured on the low-shear plateau. Measurements obtained with a rheometer (Anton Paar, MCR 302 A) using a cone-plate geometry are shown in Fig. 8.

We can observe a shear-thinning behavior reminiscent of that of long-chained polymers that tend to reduce the bulk viscosity when the entanglement of the chains are minimized at a high shear rate. The maximum shear rate in the system is at the wall of the nozzle exit and can be calculated from the Poiseuille flow:

$$\dot{\gamma} = \frac{32Q_{\mathrm{d}}}{\pi {d_{\mathrm{core}}}^3}, \tag{4}$$

where d_{core} is the diameter of the nozzle exit for the core phase (equal to 30 μm and 90 μm for SN and LN, respectively). Using Q_{d} values from Table 2, we find intervals of $[2.5, 6.3] \times 10^4\ \mathrm{s}^{-1}$ for the maximum shear rate for the experiments involving the small nozzle. The instrument used did not allow reaching such high shear rates with the low viscosity alginate but we can assume that either we are still in the Newtonian regime or closely passed the transition to the shear thinning regime. For the large nozzle, the maximum shear rates of the reported experiments lie in the interval $[1.3, 23] \times 10^3\ \mathrm{s}^{-1}$. For these values of the shear rate, solutions are either at the transition between the Newtonian regime at low shear rate and the shear-thinning one, or just above. Note that the shear thinning behavior, which corresponds to a decrease of the viscosity with an increase of the shear rate, facilitates the generation of a double emulsion at high flow rates. However, within the shear ranges explored in our experiments, the variations of the viscosities are rather small and we assume that the values of the viscosity for the Newtonian regime reported in Table 1 are reasonable for all cases.

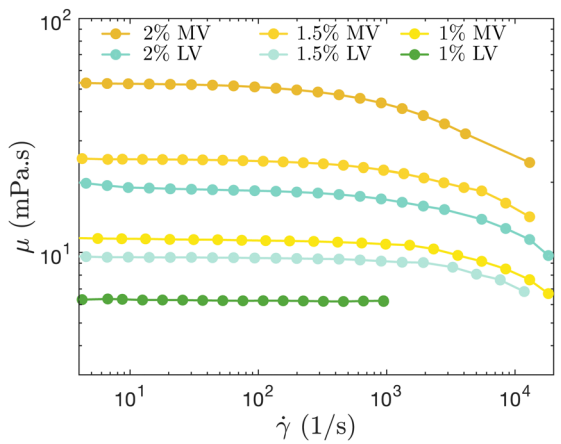

Fig. 8 Bulk shear viscosities as a function of the shear rate for the different solutions used in this study.

B Chelate-free fabrication of alginate beads

Alginate beads are fabricated through the generation of droplets of 0.5 wt% of FITC-labelled alginate solution in a continuous phase of acetic acid loaded with calcium ions,[28] using a T-junction (Upchurch, Idex). The oily continuous phase loaded with calcium is prepared by mixing $CaCl_2$ in 1-butanol at 10% w/w ratio. The mixture is added to an equal volume of oleic acid and placed on a 120 °C hot plate to evaporate butanol. The mixture is then sonicated for one hour to suspend calcium in the oil phase. Alginate beads are recovered in a bath of continuous phase and are directly imaged in this medium using a fluorescence microscope.

Acknowledgements

We thank Adam Chafaï for the support in printing glass slides with the FEMTOprint equipment. J. C. acknowledges support by F.R.S.-FNRS under the research grants CR no. 40017301 "G.El.In.Flow". This project has received funding from 747 Fédération Wallonie-Bruxelles (ARC ESCAPE project). L. E. thanks the F.R.S.-FNRS for FRIA financial support. J. M. thanks the F.R.S.-FNRS for financial support. B. S. is research director at FNRS.

Notes and references

1 M. E. Allen, J. W. Hindley, D. K. Baxani, O. Ces and Y. Elani, *Nat. Rev. Chem.*, 2022, **6**, 562–578.
2 H. Ahmed and B. T. Stokke, *Lab Chip*, 2021, **21**, 2232–2243.
3 M. Mohajeri, M. Eskandari, Z. S. Ghazali and H. S. Ghazali, *Biomed. Phys. Eng. Express*, 2022, **8**, 022001.
4 D. Lee, S. E. Greer, M. A. Kuss, Y. An and A. T. Dudley, *Biomed. Microdevices*, 2021, **23**, 1–11.
5 D. Jain and D. Bar-Shalom, *Drug Dev. Ind. Pharm.*, 2014, **40**, 1576–1584.
6 A. Łetocha, M. Miastkowska and E. Sikora, *Polymers*, 2022, **14**, 3834.
7 Y. Qin, G. Zhang and H. Chen, *J. Nutr. Food Sci.*, 2020, **3**, 100013.
8 S. Jung, R. Song, J. Kim, J. H. Ko and J. Lee, *Langmuir*, 2020, **36**, 1515–1522.

9 J. Cappello, J. Rivero-Rodríguez, Y. Vitry, A. Dewandre, B. Sobac and B. Scheid, *J. Fluid Mech.*, 2023, **956**, A21.
10 G. Fundueanu, E. Esposito, D. Mihai, A. Carpov, J. Desbrieres, M. Rinaudo and C. Nastruzzi, *Int. J. Pharm.*, 1998, **170**, 11–21.
11 J. Xie and C.-H. Wang, *J. Colloid Interface Sci.*, 2007, **312**, 247–255.
12 D. Serp, E. Cantana, C. Heinzen, U. Von Stockar and I. Marison, *Biotechnol. Bioeng.*, 2000, **70**, 41–53.
13 Y. Senuma, C. Lowe, Y. Zweifel, J. Hilborn and I. Marison, *Biotechnol. Bioeng.*, 2000, **67**, 616–622.
14 B. B. Paulo, F. D. M. Ramos and A. S. Prata, *J. Food Process Eng.*, 2017, **40**, e12591.
15 K. V. R. Reddy, J. Gupta and P. Izharuddin, *J. Drug Delivery Ther.*, 2019, **9**, 774–781.
16 K.-S. Huang, Y.-S. Lin, C.-H. Yang, C.-W. Tsai and M.-Y. Hsu, *Soft Matter*, 2011, **7**, 6713–6718.
17 C.-H. Choi, J.-H. Jung, Y. W. Rhee, D.-P. Kim, S.-E. Shim and C.-S. Lee, *Biomed. Microdevices*, 2007, **9**, 855–862.
18 Y. Morimoto, W.-H. Tan, Y. Tsuda and S. Takeuchi, *Lab Chip*, 2009, **9**, 2217–2223.
19 S. Akbari and T. Pirbodaghi, *Microfluid. Nanofluid.*, 2014, **16**, 773–777.
20 V. L. Workman, S. B. Dunnett, P. Kille and D. Palmer, *Biomicrofluidics*, 2007, **1**, 014105.
21 H. Shintaku, T. Kuwabara, S. Kawano, T. Suzuki, I. Kanno and H. Kotera, *Microsyst. Technol.*, 2007, **13**, 951–958.
22 D. Saeki, S. Sugiura, T. Kanamori, S. Sato and S. Ichikawa, *Lab Chip*, 2010, **10**, 2292–2295.
23 Q.-Q. Liao, S.-K. Zhao, B. Cai, R.-X. He, L. Rao, Y. Wu, S.-S. Guo, Q.-Y. Liu, W. Liu and X.-Z. Zhao, *Sens. Actuators, A*, 2018, **279**, 313–320.
24 A. Sattari, S. Janfaza, M. Mashhadi Keshtiban, N. Tasnim, P. Hanafizadeh and M. Hoorfar, *ACS Omega*, 2021, **6**, 25964–25971.
25 S. Utech, R. Prodanovic, A. S. Mao, R. Ostafe, D. J. Mooney and D. A. Weitz, *Adv. Healthcare Mater.*, 2015, **4**, 1628–1633.
26 Q. Chen, S. Utech, D. Chen, R. Prodanovic, J.-M. Lin and D. A. Weitz, *Lab Chip*, 2016, **16**, 1346–1349.
27 S. Damiati, *Macromol. Res.*, 2020, **28**, 1046–1053.
28 M. Lian, C. P. Collier, M. J. Doktycz and S. T. Retterer, *Biomicrofluidics*, 2012, **6**, 044108.
29 M. Y. Hwang, S. G. Kim, H. S. Lee and S. J. Muller, *Soft Matter*, 2017, **13**, 5785–5794.
30 K. Liu, H.-J. Ding, J. Liu, Y. Chen and X.-Z. Zhao, *Langmuir*, 2006, **22**, 9453–9457.
31 L. Zhao, L. Pan, K. Zhang, S. Guo, W. Liu, Y. Wang, Y. Chen, X. Zhao and H. Chan, *Lab Chip*, 2009, **9**, 2981–2986.
32 K. Liu, Y. Deng, N. Zhang, S. Li, H. Ding, F. Guo, W. Liu, S. Guo and X.-Z. Zhao, *Microfluid. Nanofluid.*, 2012, **13**, 761–767.
33 W. Jiang, M. Li, Z. Chen and K. W. Leong, *Lab Chip*, 2016, **16**, 4482–4506.
34 F. Chen, Y. Zhan, T. Geng, H. Lian, P. Xu and C. Lu, *Anal. Chem.*, 2011, **83**, 8816–8820.
35 W.-H. Tan and S. Takeuchi, *Adv. Mater.*, 2007, **19**, 2696–2701.
36 A. Rodríguez, D. Rodríguez, A. Moraleda, I. Bravo, E. Moreno and A. Notario, *Atmos. Environ.*, 2014, **96**, 145–153.
37 W.-T. Tsai, *J. Hazard. Mater.*, 2005, **119**, 69–78.
38 S. Saji, A. Hebden, P. Goswami and C. Du, *Sustainability*, 2022, **14**, 5181.
39 P. E. Ramos, P. Silva, M. M. Alario, L. M. Pastrana, J. A. Teixeira, M. A. Cerqueira and A. A. Vicente, *Food Hydrocolloids*, 2018, **77**, 8–16.
40 X. Yang, H. Sui, H. Liang, J. Li and B. Li, *Front. Nutr.*, 2022, **8**, 1217.
41 I. Ben Djemaa, F. Boulmedais, S. Auguste, M. Tarnowska, S. Andrieux and W. Drenckhan-Andreatta, *Langmuir*, 2024, DOI: **10.1021/acs.langmuir.3c03959**.
42 C. Rolsky and V. Kelkar, *Int. J. Environ. Res. Public Health*, 2021, **18**, 6027.
43 D. Byrne, G. Boeije, I. Croft, G. Hüttmann, G. Luijkx, F. Meier, Y. Parulekar and G. Stijntjes, *Tenside, Surfactants, Deterg.*, 2021, **58**, 88–96.
44 C. Le Berre, P. Serp, P. Kalck and G. P. Torrence, *Ullmann's Encycl. Ind. Chem.*, 2000, 1–34.
45 A. Thomas, B. Matthäus and H.-J. Fiebig, *Ullmann's Encycl. Ind. Chem.*, 2000, 1–84.
46 M. Beltyukova, P. Kuryntseva, P. Galitskaya, S. Selivanovskaya, V. Brusko and A. Dimiev, *Horticulturae*, 2023, **9**, 623.
47 A. Dewandre, J. Rivero-Rodriguez, Y. Vitry, B. Sobac and B. Scheid, *Sci. Rep.*, 2020, **10**, 1–17.
48 M. Mettler, A. Dewandre, N. Tumanov, J. Wouters and J. Septavaux, *Chem. Commun.*, 2023, **59**, 12739–12742.
49 Y. Vitry, J. Septavaux, A. Dewandre and B. Scheid, *Method to encapsulate an aqueous solution comprising a compound of interest in a matrix*, *US Pat.*, 18/246,005, 2023.
50 L. Biom, C. Umr and L. Roberval, *Francais Mec*, 2009, pp. 1–6.
51 J. Zhong, Y. Yang, L. Liao and C. Zhang, *Biomater. Sci.*, 2020, **8**, 2734–2755.
52 M. Riaz, M. Versaevel, D. Mohammed, K. Glinel and S. Gabriele, *Sci. Rep.*, 2016, **6**, 34141.
53 J. Lantoine, T. Grevesse, A. Villers, G. Delhaye, C. Mestdagh, M. Versaevel, D. Mohammed, C. Bruyere, L. Alaimo and S. P. Lacour, *et al.*, *Biomaterials*, 2016, **89**, 14–24.
54 D. Mohammed, M. Versaevel, C. Bruyère, L. Alaimo, M. Luciano, E. Vercruysse, A. Procès and S. Gabriele, *Front. Bioeng. Biotechnol.*, 2019, **7**, 162.
55 J. Wu, S. Yadavali, D. A. Issadore and D. Lee, *Adv. Mater. Technol.*, 2022, **7**, 2101160.
56 J. E. Mealy, J. J. Chung, H.-H. Jeong, D. Issadore, D. Lee, P. Atluri and J. A. Burdick, *Adv. Mater.*, 2018, **30**, 1705912.

